CONF-9009261--3

Electronic excitations in fast ion-solid collisions

Joachim Burgdörfer
Department of Physics and Astronomy,
University of Tennessee, Knoxville, TN 37996
and
Oak Ridge National Laboratory, Oak Ridge, TN 37831, USA

CONF-9009261--3

DE91 000736

Abstract

We review recent developments in the study of electronic excitation of projectiles in fast ion-solid collisions. Our focus will be primarily on theory but experimental advances will also be discussed. Topics include the evidence for velocity-dependent thresholds for the existence of bound states, wake-field effects on excited states, the electronic excitation of channeled projectiles, transport phenomena, and the interaction of highly charged ions with surfaces.

I. Introduction

Since the advent of the so-called "beam foil" spectroscopy almost three decades ago, an impressive amount of data[1] has been accumulated on the production of charge states and excitation states, both bound and continuum states, produced by the transmission of atoms and ions through solids. A complex array of interaction processes produces a variety of excited, sometimes "exotic", configurations not easily accessible by other means. This is to be contrasted with excitation by photons which is limited by stringent selection rules. Despite the extensive application of the ion-solid interaction as a spectroscopic tool and as an efficient ionizing agent ("stripper"), a microscopic understanding of the dynamics of the excitation process, of the evolution and transport of electrons accompanying fast ions, has been rather limited. Many fundamental questions concerning the existence, the modes of formation, and the lifetime of excited states first noted by Bohr and Lindhard[2] in their classic paper from 1954 are still unanswered. These difficulties result from the complexity of the interaction, from the importance of multiple scattering and from the fact that relevant perturbations are often sufficiently strong as to preclude a perturbational treatment. In recent years, however, considerable progress has been made in the theory of ion-solid collisions, in particular, since high-speed large scale computations allow an increasingly realistic simulation of the transient electronic dynamics. While these efforts are still in their infancy, they have already provided considerable insight into "what is going on" inside the solid.

To set the stage, Fig. 1 shows the evolution of the electron density as a proton approaches, penetrates, and finally exits a thin "foil." This calculation is performed in a time-dependent Hartree Fock (TDHF) approximation[3]. The foil is modelled by a slab of "jellium", i.e., an electron gas confined by a uniform positive background potential with sharp edges located at $z = \pm 10$a.u. with 20 a.u. thickness and a lateral extension of 40 a.u. The speed of the protons equals the Fermi velocity

$$v_F = (3\pi^2 N_e)^{1/3}, \tag{1}$$

the characteristic speed of the electron gas having density N_e. The unperturbed electron gas displays density oscillations (Friedel oscillations) inside the slab and an exponentially decaying tail of tunneling electron into the vacuum (Fig. 1a). Both are consequences of the quantum mechanical response of the electronic density to the presence of the surface potential step. As the proton approaches the surface (Fig. 1b) charge exchange by resonant tunneling into the Coulomb well of the proton sets in at rather large distances. At the same time density fluctuations in the target ("plasma oscillations") with plasmon

$$\omega_p = (4\pi N_e)^{1/2} \tag{2}$$

Our focus will be primarily on the description of projectile centered states since here both experiment and theory are far more advanced. However, the recent observation[4] of electronic shock waves in the target is noteworthy. The density fluctuations trailing the ion are expected[5] to be confined within a Mach cone with cone angle

$$\theta_{cone} \simeq \cos^{-1}(v_F/v_P). \tag{3}$$

As the cone approaches the surface preferential low energy electron emission with $v_e \lesssim v_F$ is expected in a direction perpendicular to the shock wave front. The peak in the angular distribution of slow secondary electrons (Fig. 2) emitted by N^+ penetrating a thin foil of thickness $d = 1890$ a.u. ($v_P = 2.4$ a.u.) have been attributed to the emission of shock electrons. Their identification relies on the dependence of the peak angle on the collision velocity (Eq. 3). These data appear to be the first direct and detailed evidence for "collective" target excitations by fast ions. The well known plasmon loss peaks have been observed, up to now, only for electron transmission[6].

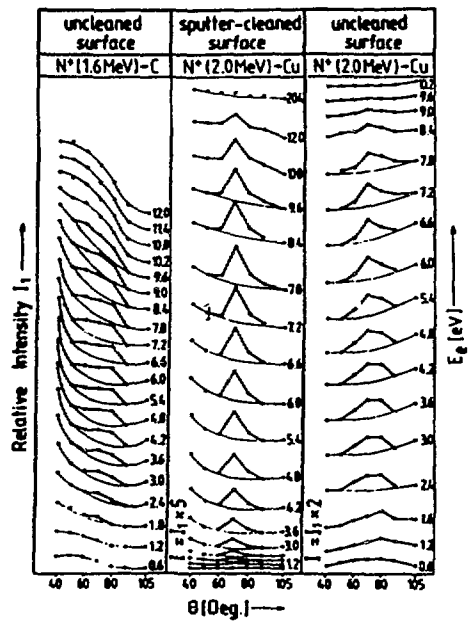

Fig. 2. Angular distributions ($40^o \leq \theta \leq 105^o$) of low-energy secondary electrons at different electron energies ($0.072 \leq E \leq 0.75$) from a C foil ($d = 1890$ a.u., left), and a Cu foil ($d = 1890$ a.u.) sputter-cleaned (center) and uncleaned (right), from Ref. 4.

In Sect. II we introduce basic concepts of the theory of projectile excitation in dense media and present simple-minded order-of-magnitude estimates in order to extract characteristic parameters of the problem. In later sections we will fill in on this physical picture with help of a few examples such as velocity dependent thresholds, dynamical screening, channeling, transport, and surface effects. In accordance with the guidance given to the authors by the organizers of this conference I will attempt to deemphasize the presentation of work from our group. Nonetheless, my selection of examples is far from being representative and inadvertently biased towards topics of my own interest. Atomic units will be used throughout unless stated otherwise.

II. Basic Concepts

The electronic evolution associated with the penetration of fast ions through matter is an extremely complex many-body scattering problem for which even the construction of the appropriate Schrödinger (or Lippmann-Schwinger) equation is a highly non-trivial task, let alone its solution at any satisfactory level. Drastic simplification based on intuition and hand-waving arguments have to be invoked in order to set up a tractable problem which, in turn, may be accessible to an approximate solution. The first step along the route of simplification concerns the translational degrees of freedom of the projectile. Since the mass ratio of electronic to nuclear mass $1/M \leq 10^{-3}$ is exceedingly small, the projectile ion is assumed to follow a classical constant-velocity trajectory

$$Z = v_p t, \tag{4}$$

neglecting thereby rare hard collisions with the ionic cores of the target. The projectile is assumed to be fast, i.e.

$$v_p >> v_F \simeq 1. \tag{5}$$

In cases where we want to employ perturbation theory for electronic transitions, the criterion (5) is sufficient only when electronic inner shell processes can be neglected. More rigorously, we should require

$$v_p \gtrsim v_K \tag{6}$$

where $v_K (\simeq Z_{p,T})$ is the orbital velocity of the K shell of the projectile or target, respectively.

Turning now to important parameters characterizing the bound state of the projectile, the binding energy (in hydrogenic approximation) is given by

$$\epsilon = -q^2/2n^2 \tag{7}$$

where q is the charge state of the ion. Heavy ions possess a charge state distribution characterized by a mean charge state $\bar{q}$ which may be different inside and outside the solid. Using a Thomas-Fermi model a phenomenological relation between $\bar{q}$, the nucleus charge Z_p and v_p can be found[7]

$$\bar{q} = Z_p(1 - \exp(-v_p/Z_p^{2/3})). \tag{8}$$

Other important parameters are the classical orbital frequency (or, quantum mechanically, the level spacing),

$$\omega_n = \frac{d\epsilon}{dn} = \frac{q^2}{n^3}, \tag{9}$$

and the orbital radius

$$< r >_n \simeq 3n^2/2q. \tag{10}$$

Projectile states are, in fact, not bound states but quasi-bound states, i.e. resonances in the continuum since they are subject to collisional destruction or radiative decay. Decay rates (inverse lifetimes) for radiative decay are of the order of

$$\Gamma_r = \frac{1}{\tau_r} \simeq \alpha^3 q^4/n^3, \tag{11}$$

($\alpha = 1/137$ the Sommerfeld fine structure constant) while an order-of-magnitude estimate (upper limit) for the collisional broadening of the state is given by the collision frequency of a free electron,

$$\Gamma_c = \frac{1}{\tau_c} = \frac{v_p}{\lambda_f} \tag{12}$$

where λ_f is the mean free path (mfp) of the free electron in the medium. For deeply bound states (Eq. 12) overestimates the collisional loss rate. The mfp is the characteristic parameter for the collisional perturbation by the solid. It contains contributions from elastic scattering at the ionic target cores (λ_{el}) and the inelastic electron-electron scattering (λ_{in}):

$$\lambda_f^{-1} = \lambda_{el}^{-1} + \lambda_{in}^{-1}. \tag{13}$$

As an estimate for λ_{el} we can use[8]

$$\lambda_{el} \simeq \frac{v_p^2/a_{TF}^2 + \epsilon_n^2}{4\pi Z_T^2 N_T} \tag{14}$$

where $a_{TF} \approx 0.885\, Z_T^{-1/3}$ is the Thomas-Fermi screening length (Z_T= nuclear charge of the target atom) and N_T is the number density of the target. (For monovalent targets, $N_T = N_e$). Eq.(14) is derived under the assumption of a quasi-free electron and is therefore not valid for small n. In the Rydberg limit, $n \to \infty$, Eq.(14) reduces to

$$\lambda_{el} \simeq v_p^2/(4\pi Z_T^2 a_{TF}^2 N_T) \tag{15}$$

The contribution to the mfp originating from inelastic collisions between the projectile electron and the valence electrons of the target can be estimated to be of the order of

$$\lambda_{in} \simeq \frac{v_p^2}{\omega_p^2 ln\left(\sqrt{\frac{2}{\omega_p}} v_p\right)}. \tag{16}$$

In addition to the mfp (or, equivalently, the collision frequency), individual collisions are characterized by the collision time, the duration of the collisional perturbation which is of the order of

$$\Delta t_c \simeq a_{TF}/v_p. \tag{17}$$

with $\Delta t_c << \tau_c$. The nearest neighbor spacing of target atoms is of the order of

$$d \simeq N_T^{-1/3} \simeq 5\, a.u. \tag{18}$$

For propagation in amorphous media or in "random" directions of a crystal, the sequence of collisions is a stochastic random process with no well-defined time structure. For channeling in single crystals the (soft) collisional interaction with the lattice sites becomes periodic with frequency

$$\omega_{res} = 2\pi\, v_p/d \tag{19}$$

while the collisions with the electrons in the channel remain a stochastic process. Under channeling conditions $\lambda_{el}^{-1} \simeq 0$.

The interaction with the target electrons (treated as an "electron gas") has another profound effect: The collective response of the electron gas to the Coulomb field of the projectile leads to dynamical screening characterized by the dynamical screening length

$$\lambda_D = v_p/\omega_p. \tag{20}$$

For low v_p, the projectile velocity should be replaced by the Fermi velocity v_F in (20) defining the static screening length of the electron gas. The latter is somewhat larger than a_{TF} reflecting the fact that the valence electron density is smaller than the total electron density near the core. The effective potential due to dynamical screening, V_{sc}, (Fig. 3) reduces the binding energy of the projectile states and supports only a finite number of bound states due to its asymptotically short-ranged character. Furthermore it possesses an oscillatory wake which allows for the existence of exotic, non-atomic

quasi-bound states of "wake-riding electrons."[9-11] The qualitative similarity between the dynamical screening potential (Fig. 3) calculated in plasmon-pole approximation for the dielectric function for an infinite medium and the density fluctuations calculated in the TDHF approximation for a jellium slab (Fig. 1), is quite remarkable in view of the vast differences in the underlying approaches.

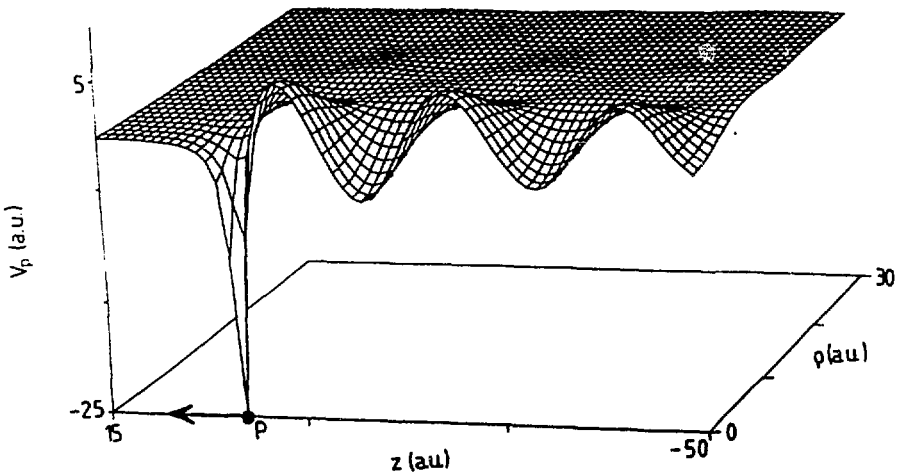

Fig. 3. Dynamical screening potential of S^{16+} in Al calculated in plasmon-pole approximation to the dielectric function ($v_p = 1$ a.u.).

We can now give a few order-of-magnitude estimates characterizing the production and evolution of projectile states inside the solid. Answering the most fundamental question to what extent excited states exist, if at all, several criteria have to be considered. The criterion most frequently discussed in literature is geometric in nature. The size of the orbital (Eq. 10) should not exceed the lattice spacing (Eq. 18),

$$3\frac{n^2}{q} \lesssim d, \tag{21}$$

thereby defining a cut-off quantum number

$$n_g \simeq \sqrt{dq/3} \tag{22}$$

above which bound states no longer "fit" inside the solid. We emphasize that (22) is neither necessary or sufficient since the stability of the electronic motion is determined by the dynamical processes, in particular, by the strength of the perturbation and the availability of open decay channels. The well known exciton states in semiconductors (in the static limit $v_p \to 0$) with diameters encompassing many lattice sites attests to the dynamic nature of stability limits.

Taking dynamical screening into account quasi-bound states cease to exist when the dynamical screening length and the radius of the orbital become comparable. Using (20) as characteristic length within which the Coulomb potential is altered we find

$$\frac{v_p}{\omega_p} \simeq \frac{3}{2}\frac{n^2}{q^2}, \tag{23}$$

or a critical quantum number

$$n_b \simeq (2v_p\, q/3\omega_p)^{1/2} \tag{24}$$

above which bound states no longer exist because of screening. In addition we can find a more stringent criterion for the existence of well-defined discrete bound states. We require that collisional broadening should not exceed the level spacing. Using for the latter the distance between energy shells (Eq. (9)), we find with help of Eqs. (12, 13),

$$\omega_n = \Gamma_c \tag{25}$$

or

$$n_c \simeq \left[\frac{q^2\, v_p}{\omega_p^2} ln \left(\sqrt{\frac{2}{\omega_p}} v_p \right) \frac{1}{1 + \frac{3.1\pi Z_T^{4/3} N_T}{\omega_p^2} ln \left(\sqrt{\frac{2}{\omega_p}} v_p \right)} \right]^{1/3} . \tag{26}$$

Eqs. (24) and (26) allow therefore to divide the projectile state space into different regions (Fig. 4): discrete core states ($n < n_c$) which closely resemble moderately perturbed atomic states, a continuum of negative energy states ($n_c < n < n_b$) which, in general, will be strongly perturbed having little resemblance to asymptotic stationary states, and finally a positive-energy continuum ($n > n_b$). On grounds of the Bohr correspondence principle, classical dynamics is expected to be valid for large quantum numbers, $n >> 1$ (more rigorously, all quantum numbers involved should be large). In the present case of a bound state spectrum embedded into a continuum via strong collisional coupling ($n > n_c$) , more complex considerations concerning the noise-driven quantum dynamics apply[12]. As a crude estimate we can use n_c (Eq. 26) as the classical-quantum border.

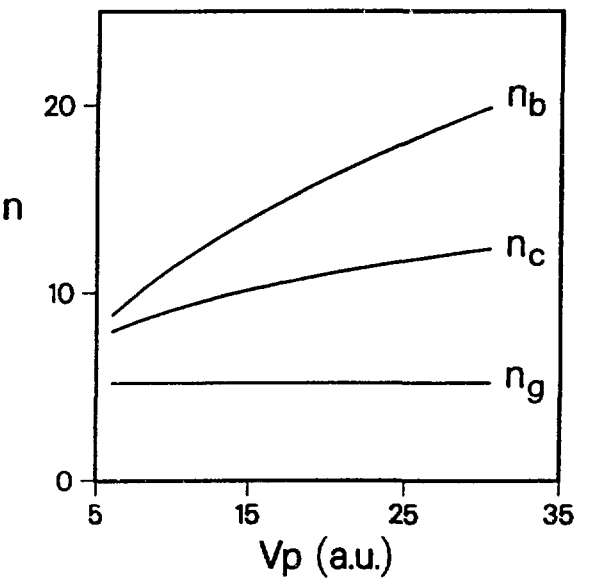

Fig. 4. Decomposition of excited state manifolds around a fast sulphur ion S^{16+} in a carbon foil as a function of v_p; n_c : classical-quantum border (Eq. 26); n_b: border of bound (negative energy) states (Eq.24); n_g: geometric border (Eq. 22). Only an order-of-magnitude estimate is given.

For core states we can, furthermore, distinguish between states quenched primarily by collisions and states decaying radiatively. The border is given by

$$\Gamma_c \simeq \Gamma_r. \tag{27}$$

or

$$n_r \simeq \left[\frac{\alpha^3 q^4 v_p}{\omega_p^2} ln \left(\sqrt{\frac{2}{\omega_p}} v_p \right) \frac{1}{1 + \frac{3.1\pi Z_T^{4/3} N_T}{\omega_p^2} ln \left(\sqrt{\frac{2}{\omega_p}} v_p \right)} \right]^{1/3}. \tag{28}$$

For $n < n_r$ radiative decay dominates over collisional destruction.

The evolution of core states can be described by rate equation models[13,14] (i.e., discrete master equations) with only a modest number of states included. The transition rates (W_{ij}) in the rate equation for the probability distribution P_i,

$$v_p \frac{dP_i}{dZ} = \sum_j (W_{ij} P_j - W_{ji} P_i) \tag{29}$$

are given in terms of atomic cross sections $\sigma_{j,i}$

$$W_{ij} = v_p N_T \sigma_{j,i}. \tag{30}$$

The channel indices (ij) in (29) refer to either different excited states of a given charge state or different charge states. Accordingly, $\sigma_{j,i}$ refer to the corresponding atomic cross sections for excitation, ionization, electron capture etc. The loss of phase coherence underlying the master equation (29) is due to the stochastic character of the collision process. This description has been applied to a large number of collision systems an example of which is shown in Fig. 5. The evolution of several charge states in 125 MeV

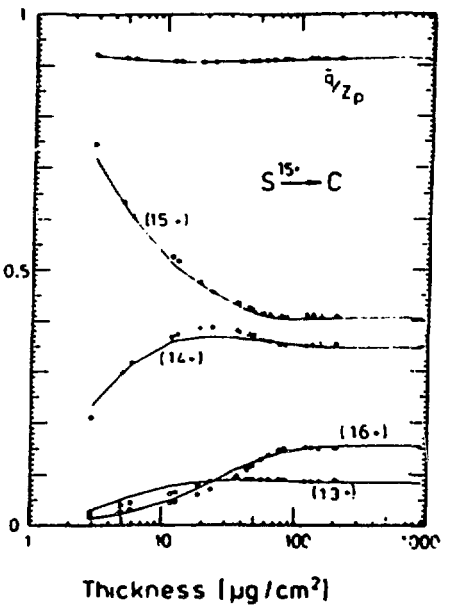

Fig. 5. Charge state of 125 MeV sulphur ions with initial charge state 15+ as a function of the thickness of carbon foil (o experiment; —— calculation), from Ref. 13.

sulphur as a function of foil thickness, i.e., as a function of distance of propagation can be traced quite accurately[13]. Limitations, however, have become apparent. Chetioui et al.[14] have reported on a perturbation of the ℓ distribution predicted by (29) due to the effective electric field produced by the anisotropic dynamical screening charge density. The atomic states in the solid are therefore Stark states. Furthermore, since this "wake" field is, to a good degree of approximation, time independent in the frame of the projectile, the characteristic interaction time is much longer (of the order of the dwell time in the solid) compared to the collision time for binary atomic collisions (Eq.17). Phase coherences due to field mixing may therefore persist and have been, indeed, observed[14].

For the formation of highly excited states beyond the border of existence of discrete quantum states ($n > n_c$) a different description of the continuous phase space distribution is needed. Within the framework of classical dynamics the electronic evolution is described by a phase space master equation for the distribution function ρ[15],

$$v_p \frac{\partial}{\partial Z}\rho(\vec{r},\vec{v},Z) = (\hat{L} + \hat{R})\rho(\vec{r},\vec{v},Z), \tag{31}$$

where the classical Liouville operator

$$\hat{L} = -\vec{v}\cdot\vec{\nabla}_r + \vec{\nabla}V_p\cdot\vec{\nabla}_v \tag{32}$$

describes the phase space flow ("drift") due to the effective electron-projectile interaction V_p and $\hat{R}$ is the collision (integral) operator describing stochastic collisions of the electrons in the solid. The phase-space coordinates $(\vec{r},\vec{v})$ refer to the projectile frame. One conceptual drawback of the classical dynamics approach is that the initial state of the electron, usually a tightly bound electron of the target or projectile, is a true quantum state. The somewhat surprising success of classical trajectory Monte Carlo (CTMC) calculations[16] in describing electronic transitions between low-lying states in ion-atom collisions indicates, however, a broader applicability of classical dynamics. An example for the application of (31) will be given in Section V.

Since in most cases the experimental observation refers to asymptotic states in the vacuum, the modification of the projectile state population upon exit from the solid plays an important role. The characteristic parameter for the transition is the transit time through the surface. For a particle exiting with angle δ relative to the surface normal the transit time t_s is of the order

$$t_s \simeq \frac{2}{v_p\cos\delta}. \tag{33}$$

For transmission problems with an outgoing trajectory close to the surface normal ($\delta \approx 0$) and high speeds the transit time is short ($t_s << 1$) compared to the orbital period ($\sim \omega_n^{-1}$, Eq. 9), except for deeply bound states. A second characteristic parameter is the strength of the surface potential. For a jellium model we have

$$V_o = W + \frac{1}{2}v_F^2 \tag{34}$$

in terms of the work function W and the Fermi energy. V_o has to be compared with the change of potential energy due to the breakdown of dynamical screening ($\sim q/\lambda_D$). The maximum strength for the time-dependent perturbation due to transit through the surface is therefore $\sim (V_o - q/\lambda_D)$. According to (33), for highly excited states the influence of the potential step can therefore be treated in sudden approximation by which the electron jumps from the potential surface of the dynamical screening potential to the bare atomic Coulomb potential in the vacuum[15]. As the transit time increases, e.g. for large angles of exit ($\delta \to \pi/2$), the influence of the surface potential

becomes important. The latter has profound effects on electronic excitation in ion-surface scattering at grazing incidence (see Sec. VI). For low-lying states, the sudden approximation may not be valid. However, in this case the time-dependent perturbation is weak. Since

$$|V_o - q/\lambda_D| << \frac{q^2}{2n^2} \tag{35}$$

for $q >> 1$ and small n, core states are little affected during the penetration of the exit surface[17].

III. Velocity dependent thresholds for the existence of excited states.

After the above qualitative overview of fundamental interaction phenomena, we turn to specific examples illustrating recent progress.

Eq. (24) implies the existence of a characteristic threshold above which a bound state no longer exists because of dynamical screening. This threshold will depend on the projectile velocity, and the charge state involved as well as on the properties of the medium. The existence of a dynamical threshold has been, in fact, predicted some time ago[7,18]. Recently, Chevallier et al.[19] have found evidence for a velocity dependent threshold for the $n = 3$ manifold in He^+ (Fig. 6). The relatively abrupt change of the velocity dependent relative population fraction, $P(He^+(3p)/P(He^+)$, in collisions with a carbon foil near $v_p = 3.7$ a.u. was attributed to a threshold for the existence of a $He^+(3p)$ state inside the solid. These authors also find that in the same velocity region, $(2 \leq v_F \leq 5)$, the $2p$ state exists everywhere while the $4p$ state is unstable over the whole interval.[20] These results can be compared with a recent comprehensive theoretical study of atomic eigenstates in the dynamical screening potential by Müller et al[21]. Using both

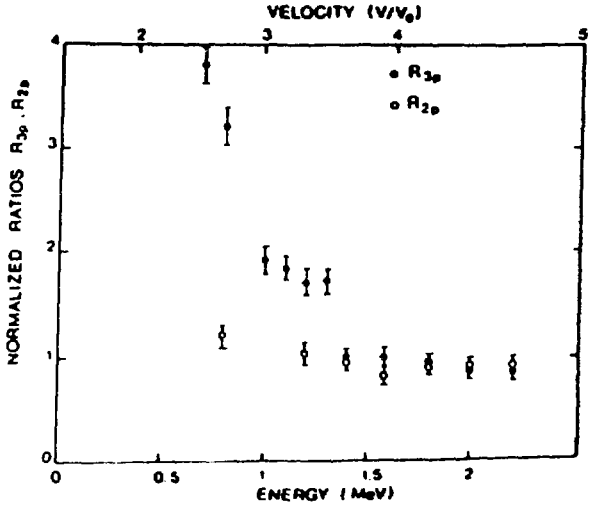

Fig. 6. Velocity dependence of ratios R, $P(He^+(3p))/(P(He^+)$ and $P(He^+(2p))$ $/P(He^+)$, normalized to unity for $v_p = 3.7$, from Ref. 19.

semiclassical Einstein-Brillouin-Keller (EBK) quantization, and diagonalization of the nonrelativistic hydrogenic Hamiltonian matrix in the truncated Hilbert space of ≈ 600 hydrogenic eigenstates of the same exact symmetry, a large number of eigenvalues have been calculated. Fig. 7 displays energy levels of the $n = 3$ manifold of the He^+

spectrum as a function of the inverse projectile velocity (i.e. proportional to the perturbation parameter q/λ_D). An excited state ceases to exist when the level is promoted to threshold

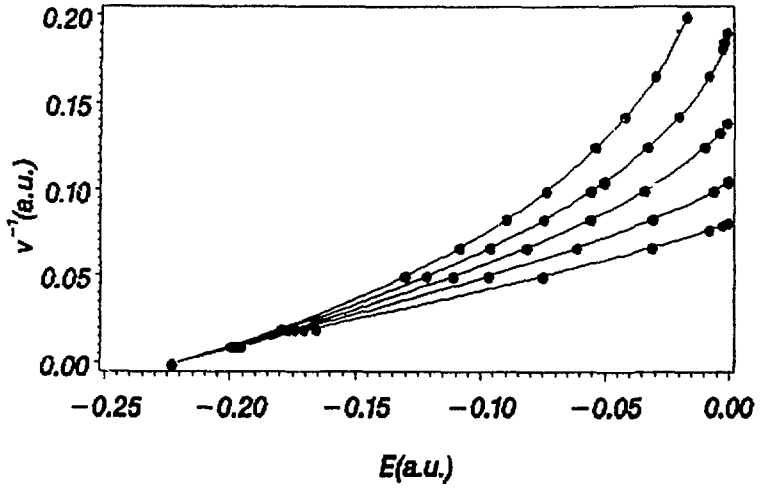

Fig. 7. Level splitting of the $n = 3$ manifolds of He^+ in carbon as a function of v_p^{-1} (proportional to perturbation parameter q/λ_D), approximate electric quantum number $k = -2, -1, 0, 1, 2$, from top to bottom.

($\epsilon = 0$). Because of a large number of avoided crossings in the vicinity of the threshold and the sudden transition upon exit (Eq. (33)) the diabatic extrapolation of the levels (avoided crossings are treated as real crossings) was used. The threshold for a given manifold is defined by the critical velocity v_c at which the last member of the manifold becomes unstable, i.e., enters the positive-energy continuum. Fig. 8 displays the critical

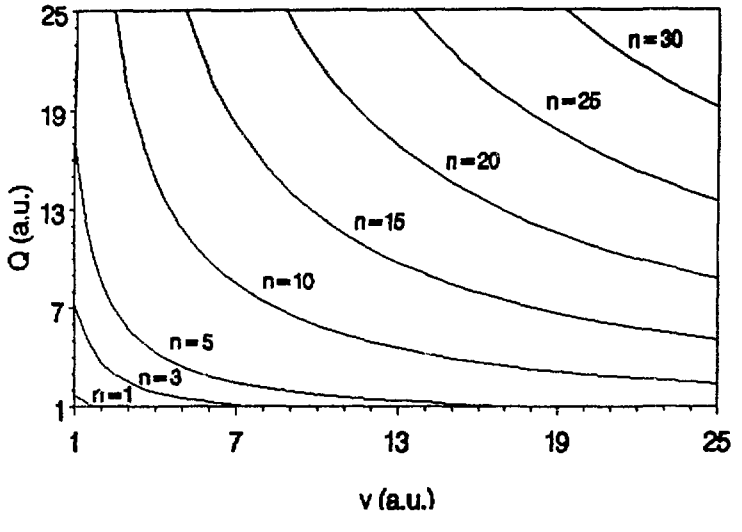

Fig. 8. Thresholds for existence of bound hydrogenic n manifolds for different charge states q and projectile speeds v_p.

threshold lines for the existence of a given manifold for different combinations of charge states and projectiles. For $He^+(q = 2)$ and $n = 3$ the threshold in carbons lies at $v_p = 3.6$a.u. in amazing agreement with the experiment. We expect this agreement to be, in part, fortuitous for several reasons: $n = 3$ manifold lies above n_c (Eq. 26). Sinc the collisional broadening (Eq. (12)). is expected to smear out any sharp threshold and poses a complication in determining an accurate threshold value. Furthermore, it appears that the experimental determination of sharp changes in population is subject to considerable uncertainty due to cascade contributions and the obstruction of the photon signal near the foil.

For small perturbation parameters (high speeds) the splitting of energy levels closely resembles the linear Stark effect (Fig. 7). The anisotropic screening charge cloud concentrated behind the ion creates an electric field with the magnitude[21]

$$F = \frac{\omega_p^2}{2v_p^2} q \ln(v_p/v_F) \tag{36}$$

near the nucleus thereby inducing Stark splitting of hydrogenic core states. This splitting has been first observed in experiments of resonant coherent excitation of channeled ions[22]. For core states of very highly charged ions, the Stark splitting

$$\Delta E_{Stark} = 3nkF/q \tag{37}$$

with the electric quantum number ($k = 0, \pm 1, \ldots, \pm(n-1),$) exceeds the level broadening $\Gamma = \Gamma_r + \Gamma_c$. The phase coherence leads in this case to quantum beats ("Stark beats") observable as intensity fluctuations of the $Ly\alpha$ radiation[14]. It should be noted that the absolute value of Stark splitting (Eq. 37) is, to first approximation, independent of q. The observation of Stark beats in highly charged ions becomes possible because of the reduction of the collisional broadening for deeply bound states (Eq. (14)).

IV. Electronic excitation of channeled ion

The most profound change in the excitation dynamics of channeled ions as compared with those propagated along "random" directions is the strong suppression of collisions between projectile centered electrons and target cores. This implies several important consequences:

(a) The elastic mean free path (Eq. 14) becomes very large (ideally, infinite). Only collisions between valence target electrons and the projectile electrons are possible.
(b) Collisional excitation and ionization displays threshold and resonance phenomena. Since the ionic cores of the target no longer act as a "reservoir" of a broad distribution in momentum and energy, only the energy ($\frac{1}{2}v_p^2$) and momentum (v_p) of valence electrons as seen in the projectile frame of reference can mediate excitation, thereby limiting the number of open channels. This property has been utilized by Datz et al.[22] to measure dielectric excitation and ionization of highly charged hydrogenic ions. The valence electron density in the channel acts like an extremely dense electron beam, as seen in the rest frame of the projectile. The space charge problem limiting the formation of a laboratory electron beam of high density is elegantly taken care of by the positive background potential provided by the target cores. If beam energy lies below the first excitation threshold,

$$\frac{1}{2}v_p^2 < \epsilon_{n=2} - \epsilon_{n=1} \tag{38}$$

the direct excitation channel is closed. However, the dielectronic excitation channel may be open near a resonance by which the energy defect to the $n = 2$ level is compensated by the capture of the impacting electron into a negative energy state of the projectile.

Experimental signatures of this two-electron process are either $2p \rightarrow 1s$ X rays or a change of the charge state ($q \rightarrow q-1$). Fig. 9 presents recent experimental data[23] for hydrogenic Titanium (Ti^{21+}) together with a solution of the rate equation (Eq. (29)). This data allows a test of the calculated dielectric capture cross section (proportional to the inverse Auger rate) for gas-phase collisions entering the rate equation. The width of the dielectronic excitation resonance is determined by the width of the momentum distribution of the valence electrons ($\approx 2v_F$). It should be noted that the second step in the dielectronic recombination, the radiative stabilization by X ray emission is suppressed relative to gas-phase collisions due to the collisional loss rate for excited states determined by λ_{in}. Consequently, dielectronic excitation in channels may result in dielectronic ionization (i.e. loss of the remaining 1s electron along the sequence $1s \rightarrow n\ell \rightarrow$ continuum) or in relaxation back to the initial charge state $Ti^{21+}(1s)$ via emission of one photon followed by collisional loss rather than in capture (Ti^{20+}, via emission of two photons). The availability of a high density electron beam in channels has been recently used by Claytor et al.[24] for a measurement of the electron impact excitation cross sections for H- and He-like Uranium at GeV energies.

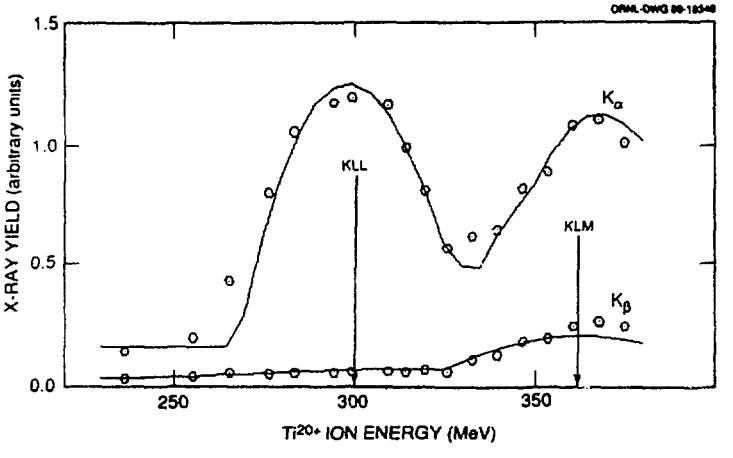

Fig. 9. Variation of the $2p \rightarrow 1s$ x ray intensity near the dielectronic resonance ($2p^2$) in Ti^{20+} as a function projectile, energy (in MeV), from Ref. 23.

As mentioned in Section II, the distant (soft) interaction of the projectile with the target atoms on regular lattice sites possesses a deterministic periodic time structure under channeling conditions (Eq. (19)). Seen in the frame of the projectile the interaction with the lattice structure acts as a coherent electric field capable of driving resonant transitions. This effect, predicted by Okorokov[25], was first unambiguously observed[22] in the resonantly modulated charge state fractions of Ni^{7+} ions as a function of the projectile when ω_{res} (or one of the higher harmonics) coincides with the excitation frequency $\omega = \epsilon_{2p} - \epsilon_{1s}$. The enhanced fraction of bare ions results from the collisional ionization prior to radiative relaxation (i.e, $\Gamma_c >> \Gamma_r$).

Recently, Kimura et al[26] have found evidence for resonant coherent excitation (RCE) in the yield of "convoy electrons". Convoy electrons correspond to near-threshold states in the continuum ($\epsilon \simeq 0$) and manifest themselves as a sharp peak ("cusp") in the forward spectrum for electron emission. The yield of convoy electrons in coincidence with carbon ions normalized to the number of exiting hydrogenic ions (C^{5+}) displays a pronounced enhancement when the ion beam velocity is tuned to the 2nd harmonic

resonance of a gold < 100 > channel (Fig. 10b). The observation of enhanced convoy electron emission for RCE allows detailed insight into the production mechanism. We note first that the thickness of the gold crystal ($\approx$ 1600Å) is large compared to the mean free path λ_{in}. Any transient enhancement has therefore decayed as the projectile reaches the exit surface. The change in convoy electron production is due to changes in preequilibrium composition of the beam near the RCE resonance.

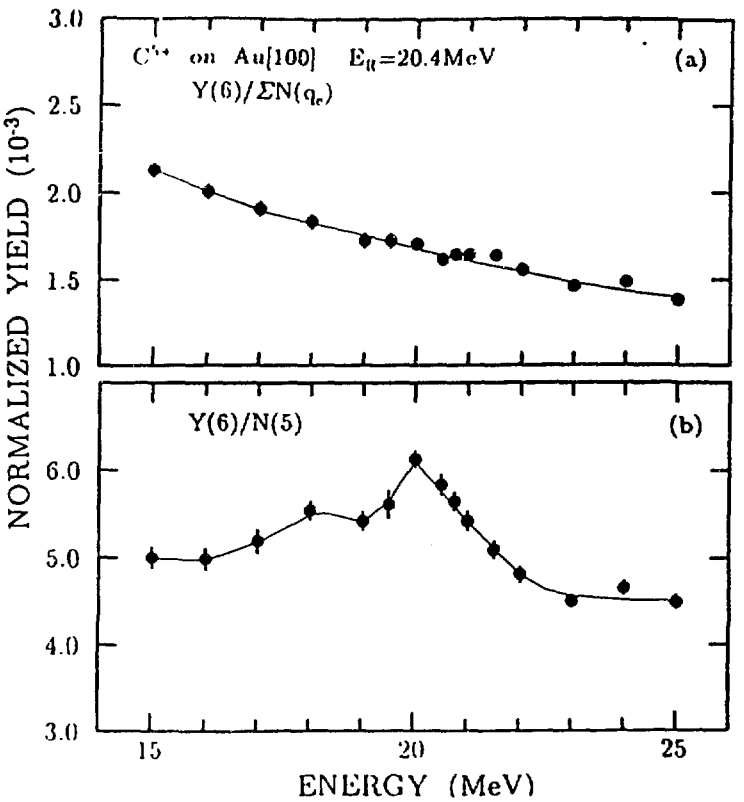

Fig. 10. Yield of convoy electrons in coincidence with outgoing C^{6+} emitted by incident C^{5+} on Au[100] near the RCE resonance. **a)** normalized to the incident beam. **b)** normalized to exiting C^{5+}, from Ref. 26.

Since the charge state distribution is far from equilibrium at the exit surface, we use the non-equilibrium solution to the master equation for the initial condition, $P^{5+}_{1s}(Z=0)=1$,

$$P^{5+}_{1s} = e^{-N_e Z(\sigma^{5+}_{1s}+\sigma^{5+}_{1s-n=2})}$$

$$P^{5+}_{n=2} = \frac{\sigma^{5+}_{1s-2}}{\sigma^{5+}_{1s}+\sigma^{5+}_{1s-2}-\sigma^{5+}_{2}} \qquad (39a\&b)$$

$$[e^{-N_e Z\sigma^{5+}_{2}} - e^{-N_e Z(\sigma^{5+}_{1s}+\sigma^{5+}_{1s-2})}],$$

where N_e refers to the electronic density in the channel, σ_n^{5+} is the electron impact ionization cross section for the n shell of C^{5+} and σ_{1s-2}^{5+} is the excitation cross section $1s \rightarrow 2s,2p$. The later will be modified by the additional RCE cross section σ_{RCE},

$$\sigma_{1s-2} \rightarrow \sigma_{1s-2} + \sigma_{RCE} \tag{40}$$

near the resonance. Eq.(39) follows from (29) if one takes only $n = 1$ and $n = 2$ core states into account and neglects all capture processes, which are small under channeling conditions, as well as deexcitation processes. The neglect of higher shells is only justified to the extent that they are not directly influenced by the resonance but only contribute to the incoherent yield.

The longstanding hypothesis[27] that convoy electron emission proceeds preferentially through electron loss from excited states can now be directly verified: Tuning through the RCE resonance, the changes in the yield of convoy electrons per incident ion (Fig. 10a) should, to a good degree of approximation, mirror the behavior of excited state fraction, F_2^{5+} (Fig. 11), but should display no correlation to either the bare ion fraction F^{6+}, or the ground state, F_{1s}^{5+}. The-at first glance-surprising observation that the "pumped" final state, $F_{n=2}^{5+}$, as well as the convoy yield (Fig 10a) show no resonant enhancement is consequence of the fact that both the total loss from excited states as well as ELC has a much larger cross section than from the ground state. Consequently, the resonant "pumping" of the $C^{5+}(n = 2)$ effectively pumps the C^{6+} charge state because of the rapid loss. Furthermore, since ELC cross sections for excited states are much larger, the depletion of the ground state is inconsequential for the convoy yield.

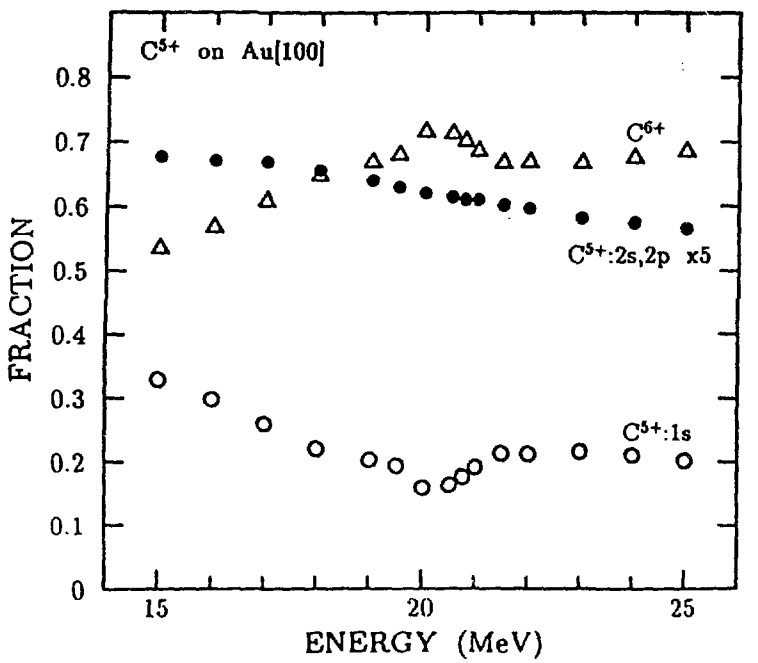

Fig. 11. Charge state (C_{1s}^{5+}, C^{6+}) and excited state $C^{5+}(n = 2)$ fraction near the RCE resonance, from Ref. 26.

We also note that the population fractions as well as the convoy yield displays a broadened resonance which is due to both collisional broadening and the Stark splitting of the $n = 2$ manifold. A comparison between convoy electron spectra for random and non-resonant channeling conditions has been recently performed at GANIL by Andriamonje et al.[28] for bare Xenon ions($q = 54$) and projectile velocities $v_p = 40\,a.u.$ One remarkable result was the expected strong suppression of electron capture to continuum under channeling conditions since mechanical capture of (quasi) free electrons is forbidden.

V. Transport processes and the production of high-ℓ states

For highly excited states beyond the border of discrete quantum states, the changes in population are described by the transport equation for the probability flow in phase space (Eq. (31)). Direct evidence for multiple scattering effects in the final projectile state population have been found in the abundance of high ℓ states absent in ion-atom collisions under otherwise similar conditions[29].

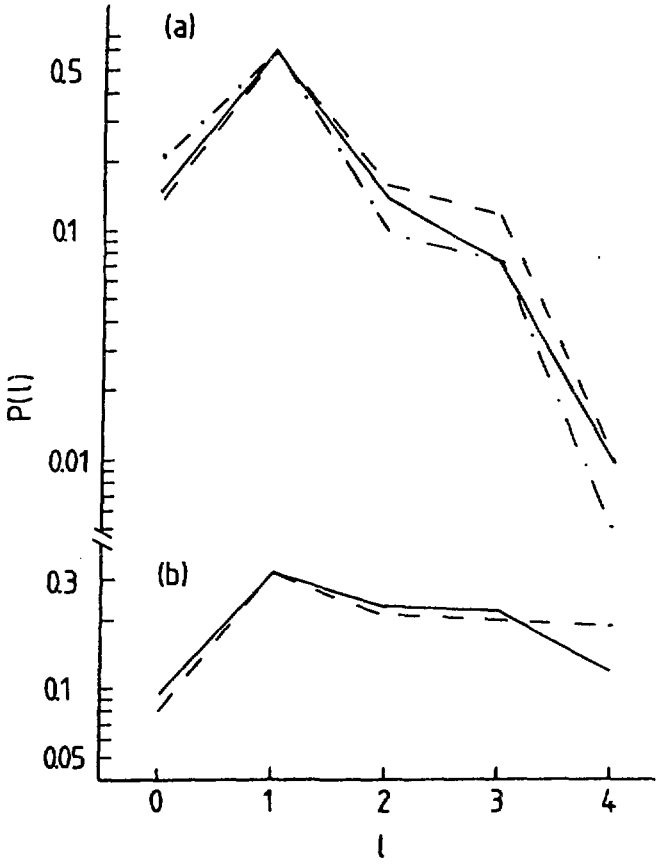

Fig. 12. ℓ-distribution $P(\ell)$ in $n = 5$ of $C^{2+}(2p5\ell)$ ($v_p = 2.25$ a.u.). **a)** - - - , experimental data (Ref. 30) for $C^{3+} + He \rightarrow C^{2+}(2p5\ell) + He^{+}$, $-\cdot-\cdot-\cdot-$, experimental data (Ref. 30) for $C^{2+} + He \rightarrow C^{2+}(2p5\ell) + He^{+}$; ——, simulated initial distribution for random walk. **b)** - - -, experimental data (Ref. 30) for $C^{2+}(2p5\ell)$ on carbon foil; ——, escape-depth-averaged (steady state) solution of the Langevin equation, from Ref. 31.

A detailed comparison between experiment and theory has recently become available for doubly excited states in carbon $C^{2+}(2p5l)$ produced in collisions with carbon foils[30]. According to Eq. (26) the $5l$ orbital lies at the experimental collision velocity $v_p = 2.2\,a.u.$, well above n_c (in fact, in the positive-energy continuum according to (24)), and the classical phase-space master equation should be applicable. Comparison with the simultaneously measured ℓ distribution for both excitation $C^{2+} \rightarrow He$ and electron capture $C^{3+} \rightarrow He$ in gas-phase collisions clearly display the shift to high-ℓ states (Fig. 12). In order to treat the ℓ evolution within the framework of transport theory[31] we have chosen an initial distribution in ℓ, also shown in (Fig. 12), which is modeled after the experimental ion-atom collision data (Fig 12). The mapping of the continuous classical ℓ distribution onto discrete quantum numbers was made with use of equally spaced bins centered around the semiclassical value $\ell + 1/2$. An equivalent method has been used for n. The resulting asymptotic stationary ℓ distribution in $n = 5$ (averaged over different escape depths) after foil exit shows astonishingly good agreement with the data. The only statistically significant deviation, by a factor $\simeq 1.5$, from the experimental data appears to occur in the g-state population.

The physical picture underlying the dramatic shift of the ℓ distribution to high ℓ states as compared to ion-atom collisions under single collision conditions is that multiple scattering of electrons during their correlated motion with the projectile embodied, in the transport equation, leads to a "diffusive"-like redistribution among ℓ states. Several experimental groups have reported on an enhanced transport depth for convoy electrons[32]. A similar diffusion in n quantum number, i.e., energy, in H^o has been recently observed by Mohagheghi et al.[33] in transmission through thin foils of a relativistic H^- beam with an energy of 800 MeV. A more detailed discussion of the solution to the transport equation for projectile electrons can be found in Ref. 15.

VI. Ion-surface collisions

Electronic excitation processes of ions approaching surfaces (ideally without even penetrating the surface) have become a field of great interest, both from the viewpoint of fundamental interactions between atomic systems and a semi-infinite many-body system and from the viewpoint of a large number of applications, notably, the properties of a confined plasma near the wall of the container and the production of level inversions with potential applications to x-ray lasers.

Recent experimental progress in this field is closely linked to the advent of sophisticated techniques for surface preparation and surface diagnostics which allow controlled scattering experiments at microscopically clear surfaces. In addition, the development of ECR and EBIS ion sources has expanded the range of available charge states of low to intermediate energy projectiles.

The dynamics of neutralization of a highly charged ion has been studied in several laboratories[34–37]. The rapid neutralization of a highly charged ion by transfer of 10 or more electrons is a true multi-electron process for which not even a first-order approximation is currently available. This flow of electrons is assumed to occur via resonant charge transfer from the conduction band of the solid to high Rydberg states, followed by stepwise relaxation by sequential Auger transitions. However, the characteristic time constant for relaxation as estimated from conventional two-electron Auger matrix elements is too slow to fill inner shells prior to impact. The disparity of time scales for resonant transfer and relaxation leads to a "bottleneck" and thereby to the formation of "hollow" atoms. Fig. 13 displays the complex satellite structure of a He-like X ray transition for Au^{17+} impinging on a Ag surface with an energy of $\approx 20\,keV$ per charge. States with up to 7 holes in the K and L shells but 5 electrons in the M shell have been observed [38]. A theoretical description of this process is, as of now, missing. Apart from the obvious difficulty in describing such a violent n electron process, a more subtle problem consists in reconciling vastly different time scales. If one accepts the notion[36]

that the multiple-step neutralization process occurs on the incoming part of the trajectory before the ion reaches the surface, the limited available time suggests that the relaxation process in a hollow atom in proximity of a surface differs dramatically from Auger decay of an isolated atom with only one or a few vacancies in inner shells. If at all realistic, electron-electron interactions ("correlations") and electron-surface interactions must

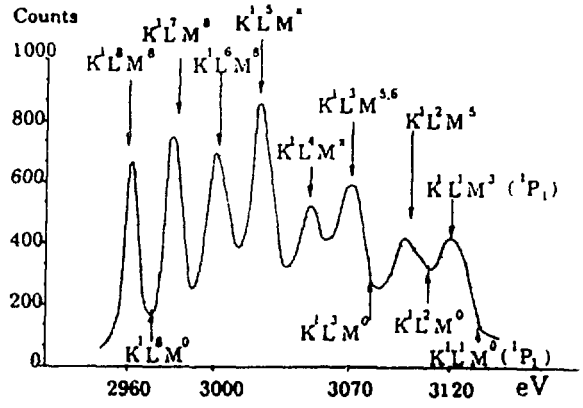

Fig. 13. $(1s2p \rightarrow (1s)^2$ x ray spectrum observed for Ar^{17+} ions impinging on Ag target, the identification of satellite lines is indicated, from Ref. 38.

play a decisive role in such a fast relaxation. Very likely, an adequate theoretical description should include quasi-resonant charge transfer between "intermediate" shells of the target and lower-lying excited states of the projectile at small distances from the surface ($\approx$0.5 to 3 a.u.). One may speculate that a classical n-body dynamics calculation which allows non-perturbative treatment of the interactions may be a promising approach to a theoretical description. The high density of states and the short time scale involved suggest that the quantal spread of the wavepacket should be of minor importance. Work along those lines is in progress[39].

Electron emission in grazing incidence collisions has recently been used in exploring the long-range interactions near the surface. Electrons emitted in ion-surface collisions have been predicted[17] to be subject to acceleration by the image potential of the accompanying ion, provided the characteristic interaction time t_s (Eq.(33)) is sufficiently long. For convoy electron emission at grazing incidence with $\delta_{ion} \approx \delta_{electron} \approx 89^o$, strong distortions due to the image potential are expected: the convoy electron peak is shifted[40,41] and broadened[42,43].

The electron in close proximity to the projectile receding from the surface is subject to the projectile potential and to the dynamical surface screening potential. The latter is given in a strongly simplified approximation by[40,44]

$$V_{image}(\vec{r}) = (2q\omega_s/v)\sin((z-vt)\omega_s/v_p)K_o\left[(\omega_s/v)[(x+x_o)^2+y^2]^{1/2}\right] \exp((z-v_pt)\gamma/4v)\theta(v_pt-z), \quad (41)$$

where K_o is the modified Bessel function, $\omega_s = \omega_p/\sqrt{2}$ is the frequency of the surface plasma, γ is the damping constant of the plasma, and θ is the step function. The projectile is assumed to travel parallel to the surface at distance x_o with velocity v_p. The effect of the electronic self-image can be, to lowest order, taken into account by

replacing $q \rightarrow (q-1)$ in (41), assuming that the average position of the electron coincides with that of the ion. Accordingly, the line shift of the convoy electron is given by

$$\Delta E \simeq \int_{x_c}^{\infty} \frac{dx_o}{\sin\theta_{out}} F_Z(x_o), \tag{42}$$

where $F_Z = -\frac{\partial}{\partial Z} V_{image}$. Fig. 14 displays recent experimental data[40] together with the estimate(Eq.(42)) for the fractional change in energy of the convoy peak $(E_o + \Delta E)/E_o$, where $E_o = v_p^2/2$ is the expected position of convoy peak. Projectile ions (H^+, He^{++}) impinge on a SnTe (001) surface at an angle of incidence of $(\theta_i = \pi/2 - \delta_i)$=6 mrad. While the quantitative agreement is poor, this model reproduces the qualitative features of the data quite well. For H^+ no peak shift is expected since $q - 1 = 0$. For He^{++} the projectile energy dependence of the peak shift is reproduced, while the magnitude is overestimated. The agreement can be improved by an ad hoc increase in the angle of the outgoing trajectory(θ_{out}) from 6 to 25 mrad. This is in accord with the observation that the electronic and projectile scattering angles do not coincide. Clearly, better quantitative agreement with the data can be expected for a theoretical treatment employing the phase space master equation (Eq. 31). The study of convoy peak shifts has been recently extended by Koyama et al.[41] to highly charged projectiles with q up to 27. Here the peak shift reaches 250 eV.

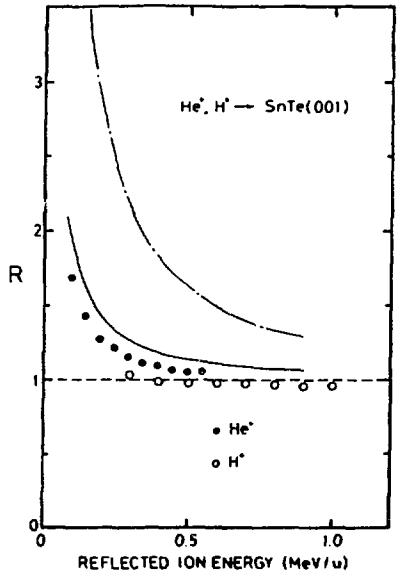

Fig. 14. Ratio of convoy electron energy position to expected convoy energy $(E_o + \Delta E)/E_o$ as a function of projectile energy (in MeV/u), angle of incidence θ_{in} = 6m mrad; o H^+ projectiles; • He^+calculations for exit angle relative to the surface $-\cdot-\cdot-$ θ_{out} = 6 mrad; and —— θ_{out} = 25 mrad, from Ref. 40.

Along similar lines, the broadening of the convoy peak can be explained in terms of an image-charge induced dipole final state interaction[42]. For large distances between the electron and the projectile, the electron moves in an effective dipole field generated by the projectile ion and its image. Employing the threshold law for a dipole ($\sim 1/r^2$)

potential, the cross section near threshold (as seen in the rest frame of the projectile) behaves as[43]

$$\frac{d\sigma}{d\epsilon} = const\, v^{-1+2\beta}, \tag{43}$$

where β depends on the angular momentum of the potential and the dipole moment. Transforming (43) to the lab frame gives a broadened cusp relative to the Coulomb cusp for all $\beta > 0$. Using β as free parameter, good agreement with the experimentally observed shape of the convoy peak has been found for $\beta \approx 0.4$, almost independent of the collision velocity.[43] This result underscores the importance of long-range potentials for the electronic excitation process in ion-surface collision.

VII. Summary

This short overview was intended to illustrate progress in the theoretical understanding of ion-solid collisions. At the same time, recent experimental advances point to the need for and to the directions of future investigations. They are motivated by both the many unsolved fundamental questions of properties of atomic systems in dense media and by their potential applications in the field of surface diagnostics, radiation damage, and coherent x ray light sources.

The author acknowledges important contributions made by many colleagues and collaborators. They include C. Bottcher, S. Elston, J. Gibbons, J. Kemmler, K. Kimura, J. Müller, I. Sellin, J. Wang and H. Winter. This work was supported in part by the National Science Foundation and by the U.S. Department of Energy, Office of Basic Energy Sciences, Division of Chemical Sciences, under Contract No. DE-AC05-840R21400 with Martin Marietta Energy Systems, Inc.

References

1. For an overview see recent proceedings of the conference series "Atomic Collisions in Solids," Nucl. Instr. Meth. B2 (1984); B13 (1986), B33 (1988), B48 (1990).
2. N. Bohr and J. Lindhard, K. Dan. Vidensk. Selsk. Mat. Fys. Medd. 28 (1954) No.7.
3. K. Schafer, N. Kwong, and J.D. Garcia, Computational Physics Communications (1990, in press).
4. H. Rothard, M. Burkhard, J. Kemmler, C. Biedermann, K. Kroneberger, P. Koschar, O. Heil, and K.O. Groeneveld, J. de Physique, 48-C9, 211 (1987).
5. W. Schäfer, H. Stöcker, B. Müller, and W. Greiner, Z. Physik A288, 349 (1978).
6. J. Ashley, J. Cowan, R. Ritchie, V. Anderson, and J. Hoelzl, Thin Solid Films 60, 361 (1979), and ref. therein.
7. See e.g., W. Brandt in Atomic Collisions in Solids, eds. S. Datz et al., (Plenum, N.Y., 1975) p. 261.
8. D. Röschenthaler et al., J. Phys. B16, L233 (1983).
9. V. Neelavathi, R. Ritchie, and W. Brandt, Phys. Rev. Lett. 33, 302 (1974).
10. J. Burgdörfer, J. Wang, and J. Müller, Phys. Rev. Lett. 62, 1599 (1989).

11. Y. Yamazaki, in Proc. of the NATO Advanced Study Institute on the Interaction of Charged Particles with Solids and Surfaces, Alicante, 1990 (Plenum Press, N.Y., 1991) in press.

12. R. Blümel et al., Phys. Rev. Lett. 62, 341 (1989).

13. H.D. Betz, R. Höppler, R. Schramm, and W. Oswald, Nucl. Instr. Meth. B33, 185 (1988).

14. J. Rozet, A. Chetioui, C. Stephan, A. Touati, D. Vernhet, and K. Wohrer, in *Proceedings of the Third Workshop on High Energy Ion-Atom Collisions*, edited by D. Berenyi and G. Hock, Lecture Notes in Physics Vol. 294 (Springer-Verlag, Berlin, 1988) p. 307.

15. J. Burgdörfer, in Ref. 14, p. 344; J. Burgdörfer and J. Gibbons, Phys. Rev. A42, 1206 (1990).

16. R. Abrines and I.C. Percival, Proc. Phys. Soc. (London) 88, 861 and 873 (1966).

17. J. Burgdörfer, Nucl. Instr. and Method. B24/25, 139 (1987).

18. J. Burgdörfer, Diploma Thesis, Freie Universität Berlin, 1978 (unpublished).

19. M. Chevallier et al., Phys. Rev. A41, 1738 (1990).

20. B. Mazuy et al., Nucl. Instr. and Meth. B31, 387 (1988).

21. J. Müller, J. Burgdörfer and D. Noid,, submitted for publication to Phys. Rev. Lett. (1990); J. Müller and J. Burgdörfer, to be published.

22. S. Datz et al., Phys. Rev. Lett. 40, 843 (1978); S. Datz, J. de Physique (Paris) C1-335 (1979).

23. S. Datz et al., Phys. Rev. Lett. 63, 742 (1989).

24. N. Claytor et al., Phys. Rev. Lett. 61, 2081 (1988).

25. V. Okorokov, JETP Lett. 2, 111 (1965).

26. K. Kimura et al., submitted for publication in Phys. Rev. Lett. (1990).

27. H. Hülskötter, J. Burgdörfer, and I. Sellin, Nucl. Instr. and Meth. B24/25, 147 (1987) and references therein.

28. S. Andriamonje et al., these proceedings.

29. H.-D. Betz, D. Röschenthaler, and J. Rothermel, Phys. Rev. Lett. 50, 34 (1983); H.-D. Betz, in Forward Electron Ejection in Ion Collisions, edited by K.O. Groeneveld et al., *Lecture Notes in Physics* Vol. 213 (Springer-Verlag, Berlin, 1984), p. 115.

30. Y. Yamazaki et al., Phys. Rev. Lett. 61, 2913 (1988).

31. J. Burgdörfer and C. Bottcher, Phys. Rev. Lett. 61, 2917 (1988).

32. I.A. Sellin, et al., in Forward Electron in Ion Collisions, *Lecture Notes in Physics*, Vol. 213 (Springer, Berlin, 1984), p. 109; R. Schramm, P. Koschar, H.-D. Betz, M. Burkhard, J. Kemmler, O. Heil, and K.O. Groeneveld, J. Phys. B18, L507 (1985); G. Schiwietz, D. Schneider, and J. Tanis, Phys. Rev. Lett. 59, 1561 (1987).

33. A.H. Mohagheghi et al., in *XVI International Conference on The Physics of Electronic and Atomic Collisions*, New York, 1989, Book of Invited Papers, eds. A. Dalgarno et al., (American Institute of Physics, N.Y., 1990), p. 487.

34. E. Donets, Nucl. Instr. and Meth. 9, 522 (1985).

35. M. Delaunay, M. Fehringer, R. Geller, P. Varga and H. Winter, Europhys. Lett.4, 377 (1987).

36. L. Folkerts and R. Morgenstern, J. de Physique 50-C1, 541 (1989).

37. D. Zehner et al. Surf. Science 178, 359 (1986).

38. J.P. Briand et al., Phys. Rev. Lett. 65, 159 (1990).

39. J. Burgdörfer to be published.

40. M. Hasegawa, K. Kimura and M. Mannami, J. Phys. Soc., Japan 57, 1834 (1988); M. Hasegawa, T. Fukuchi, T. Mizuno, K. Kimura, and M. Mannami, to be published.

41. A. Koyama et al., preprint (1990).

42. L.F. de Ferrariis and R. Baragiola, Phys. Rev. A33, 4449 (1986).

43. H. Winter, P. Strohmeier, and J. Burgdörfer, Phys. Rev. A39, 3895 (1989).

44. N. Takimoto, Phys. Rev. 146, 366 (1966).